Applied Energy 129 (2014) 373–383

Contents lists available at ScienceDirect

Applied Energy

journal homepage: www.elsevier.com/locate/apenergy

High fidelity finite difference model for exploring multi-parameter thermoelectric generator design space

Haiyan Fateh *, Chad A. Baker, Matthew J. Hall, Li Shi

Mechanical Engineering Department, University of Texas at Austin, 204 E. Dean Keeton St., Stop 2200, Austin, TX, USA

HIGHLIGHTS

- A system level numerical model for thermoelectric power generation.
- 1st and 2nd generation Mg and Mn silicide TE devices fabricated.
- The numerical model validated experimentally for power output.
- TEG module geometric design space parameters optimized numerically.
- Effects of thermal and electrical contact resistance quantified.

ARTICLE INFO

Article history:
Received 5 December 2013
Received in revised form 22 March 2014
Accepted 26 April 2014
Available online 6 June 2014

Keywords:
Thermoelectric generators
Waste heat recovery
Design optimization
Energy conversion
Magnesium silicide
Manganese silicide

ABSTRACT

Thermoelectric generators (TEGs) are being studied and developed for applications in which waste heat, for example, from the exhaust of motor vehicles is converted into usable electricity. TEGs consisting of TE elements integrated with an exhaust heat exchanger require optimization to produce the maximum possible power output. Important optimization parameters include TE element leg length, fill fraction, leg area ratio between n- and p-type legs, and load resistance. A finite difference model was developed to study the interdependencies among these optimization parameters for thermoelectric elements integrated with an exhaust gas heat exchanger. The present study was carried out for TE devices made from n-type Mg_2Si and p-type $MnSi_{1.8}$ based silicides, which are promising TE materials for use at high temperatures associated with some exhaust heat recovery systems. The model uses specified convection boundary conditions instead of specified temperature boundary conditions to duplicate realistic operating conditions for a waste heat recovery system installed in the exhaust of a vehicle. The 1st generation, and an improved 2nd generation TEG module using Mg_2Si and p-type $MnSi_{1.8}$ based silicides were fabricated and tested to compare TE power generation with the numerical model. Important results include parameter values for maximum power output per unit area and the interdependencies among those parameters. Heat transfer through the void areas was neglected in the numerical model. When thermal contact resistance between the TE element and the heat exchangers is considered negligible, the numerical model predicts that any volume of TE material can produce the same power per unit area, given the parameters are accurately optimized. Incorporating the thermal contact resistance, the numerical model predicts that the peak power output is greater for longer TE elements with larger leg areas. The optimization results present strategies to improve the performance of TEG modules used for waste heat recovery systems.

1. Introduction

Energy conservation is becoming increasingly important because of growing energy demands. This compels us to promote the development of energy efficient systems. Exhaust gases from the tail pipes of motor vehicles are responsible for dissipating roughly one third of the energy content of the fuel to the environment as heat [1–3]. Therefore, various waste heat recovery technologies are being investigated to capture that waste heat. Such technologies include organic Rankine cycles [4], turbo-compounding [5], direct use of the waste heat as thermal energy, power absorption chillers [6], and thermoelectric devices

* Corresponding author. Tel.: +1 512 471 1292.
E-mail addresses: hfateh@utexas.edu (H. Fateh), mjhall@mail.utexas.edu (M.J. Hall).

http://dx.doi.org/10.1016/j.apenergy.2014.04.088
0306-2619/

[4,7–10]. Thermoelectric devices in particular have gathered considerable attention in the last few decades. They are solid state heat engines that use the Seebeck effect to directly convert heat to electrical energy. They operate quietly, without moving parts [11], and are compact and lightweight. However, thermoelectric devices have low efficiency (<5%) in addition to being expensive; this has limited their widespread use. Nonetheless, the potential use of relatively inexpensive materials like Mg_2Si and p-type $MnSi_{1.8}$ based silicides shows promise for cost reduction and improved performance. A schematic of a typical TEG (Thermoelectric Generator) module is shown in Fig. 1. System level thermoelectric heat exchangers for waste heat recovery consist of several TEG modules integrated with a compact heat exchanger that can extract maximum heat from the exhaust flow.

Substantial research has been done in recent years regarding the design and optimization of thermoelectric heat exchangers. Applications of various thermoelectric materials exhibiting peak thermoelectric efficiencies at different temperature ranges have been studied in the past for installation in exhaust heat recovery systems [12–14]. Stobart and coworkers modeled and experimentally tested the TE performance of devices with exhaust temperatures up to 800 K. Thermal asymmetry between the hot-side and cold-side accounting for the difference in heat transfer due to internal electric energy conversion was not considered by Stobart et al. Their model was based on the average figure of merit (ZT) of the TE material that assumes optimal device geometry and optimal current [15,16]. Geometric parameters that affect TE performance include n-/p-type leg area ratio, leg length, the area of individual legs and the distance between adjacent legs. Modeling efforts by Hendricks et al. [7,10] considered temperature-dependent TE properties to determine optimal TE leg areas, lengths, and device designs. Modeling carried out by Xuan and Cheng [17–19], which dealt with thermoelectric coolers, considered the geometrical optimization of the length of TE legs only. Miller et al. studied heat transfer and heat exchanger optimization for a combined TE and organic Rankine cycle waste heat recovery system. Miller et al. calculated the TE device efficiency based on an average ZT for state of the art TE materials evaluated at typical operating temperatures [4]. A report by Wang and Dai presented an optimization study on thermoelectric generator systems for waste heat recovery in motor vehicles. They discovered that power output was more sensitive to hot side heat transfer coefficient than the cold side. They also discovered other key optimization results for TEG modules such as sensitivity of peak power to PN junction height and convection heat transfer coefficients [20]. Chen and Li et al. considered a two stage TEG module system for their study and reported optimization studies for the heat transfer surface area as well as the total number of TE elements on each TEG stage for peak power output [21]. A study by Gou, Xiao, and Yang presented a system model for low-temperature thermoelectric generators for use in waste heat recovery systems, which was verified with some experiments. An appropriate range of heat sink surface area as well as cold-side heat transfer capacity for peak power output were discussed [22]. A study by Matsubara et al. based on thermoelectric stacks composed of segmented legs projected highly efficient systems (up to 10%) [23]. Such efficiencies could produce enough power to supplement a vehicle alternator or perhaps replace it altogether [11,24]. Hussain et al. developed a model with thermally lumped TE devices that accounted for transient behavior and thermal asymmetry. In their model, the spatial variation and temperature dependence of the TE properties in individual TE devices was accounted for. Crane and coworkers developed a system level model integrating thermoelectric devices with a heat exchanger for cross-flow and counter-flow heat exchanger configurations. They used an analytical, thermally lumped TE leg performance model that correctly accounted for thermal asymmetry. Some of this modeling work was validated with experimental results. Crane's most recent model incorporated transient performance. The report also presented a novel high-power-density subassembly of the TEG module that has various advantages over the conventional TEG assembly [9,25,26]. Kumar and coworkers presented a thermal resistance based numerical model to study the electrical power output and pressure drop for various flow rates for a General Motors Co. prototype TE generator designed for a Chevrolet Suburban [27]. This study incorporated junction-averaged temperature dependent TE properties. A recent report by Espinoza and coworkers reported modeling efforts which take into account the temperature dependent properties along the heat exchanger, but not within the legs [28]. In addition, vehicle manufacturers including BMW, Ford, GM, and Ford have all been involved in studies on thermoelectric heat exchangers for automobiles in partnership with the US Department of Energy [11].

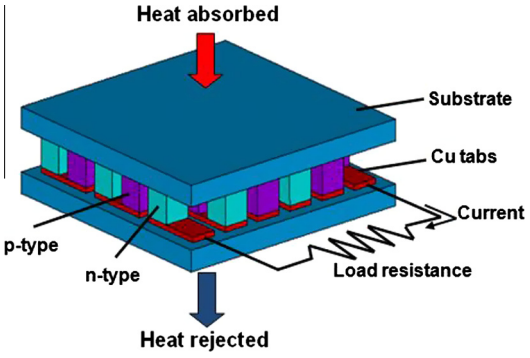

Fig. 1. Schematic of a TEG module.

Optimization studies on TEGs in the past have assumed a constant temperature boundary condition for simplified analysis. However, for a thermoelectric waste heat recovery system installed in the exhaust of a vehicle, these temperatures will be dictated by convection heat transfer on both sides (exhaust and coolant). Therefore, a more appropriate/realistic boundary condition to govern the performance of TEGs is convection heat transfer rather than constant temperature boundary conditions for TE junctions. Gomez et al. reported a modeling study incorporating constant reservoir temperatures instead of constant TE element junction temperatures. They discussed the relationship between fill fraction, leg length, and the ratio of load resistance and internal resistance for optimal performance [29]. However, their model did not account for temperature dependent TE properties. The study was carried out for low temperature ranges (~350 K) based on experimentally measured TE properties of a commercial TEG module.

None of the previous work discussed here used a TE model that accounted for spatial- and temperature-variant properties within the TE material of an individual TE couple. In addition, the majority of them have focused mainly on the optimization of the heat exchanger geometry only. The ones that discuss the optimization of TEG module geometry itself do not consider the interdependencies between the optimization variables like leg area ratio, area of individual TE legs, spacing between the legs, and the load resistance. A comprehensive study regarding the optimization of TEG modules that includes such analysis is lacking.

The present study focuses primarily on modeling the performance and optimization of TEG modules integrated with a system level heat exchanger and using Mg_2Si and p-type $MnSi_{1.8}$ based silicides as the TE materials. A numerical model was developed using a finite difference technique which accounts for spatial- and temperature- dependent thermoelectric properties. The model also couples hot-side and cold-side convection heat flux, thus

accounting for the thermal asymmetry using a numerical root finding algorithm. The model was developed to understand and analyze the interdependencies among various parameters such as the height of the TEG modules, volume of TE material, the area ratio between n-type and p-type legs, and the load resistance. The set of parameters that provide the greatest power conversion for a given heat exchanger and operating conditions is determined. In addition, two TE leg pair devices, each with a different approach to fabrication, were assembled, and an experimental setup was constructed to validate the numerical model. Electrical contact resistances have been experimentally measured and incorporated into the numerical model for validation purposes. One unique feature of this study is that it is focused on Mg and Mn silicides. These materials have potential cost advantages with comparable ZT values at higher temperatures [30], suitable for integration into heat exchangers employed in diesel and gasoline vehicles as opposed to conventional TE materials, e.g. bismuth telluride, lead telluride, and silicon germanium alloys.

2. Thermoelectric device model

To account for the temperature dependence of the TE properties in the direction of heat conduction and the thermal asymmetry, a TE device finite difference model was developed. The TE leg pairs were modeled at the device level using an iterative finite difference algorithm described by Hogan and Shih [31]. A schematic of the finite difference numerical scheme is shown in Fig. 2. The equations that govern the heat transfer and temperature distribution are:

$$\frac{\Delta T_i}{\Delta x} = \frac{1}{k_{i-1}}[JT_{i-1}\alpha_{i-1} - q_{i-1}] \tag{1}$$

$$\frac{\Delta q_i}{\Delta x} = \rho_{i-1}J^2[1 + Z_{i-1}T_{i-1}] - \frac{J\alpha_{i-1}q_{i-1}}{k_{i-1}} \tag{2}$$

In Eqs. (1) and (2), $\Delta T_i = T_i - T_{i-1}$, $\Delta q_i = q_i - q_{i-1}$, Δx is the distance between two adjacent segments, k_i is the temperature-dependent thermal conductivity evaluated in the middle of segment i, J is the electrical current density, T_i is the temperature in the middle of segment i, α_i is the temperature dependent Seebeck coefficient evaluated in the middle of segment i, q_i is the heat flux at the middle of segment i, and ρ_i is the temperature dependent electrical resistivity evaluated in the middle of segment i.

Eqs. (1) and (2) were solved for each segment of the leg.

Either load resistance or current density could be specified in the model. In this case, load resistance rather than current was input to the model since this is a parameter that needs to be specified for a given hardware configuration and can be easily controlled. Inputting load resistance rather than current, however, requires an additional set of iterations which is closed by the following equation [32]:

$$I = JA = \frac{\alpha\Delta T}{R_{load} + R_{internal}} \tag{3}$$

where A is the cross sectional area of either leg. Here, $\alpha\Delta T$ is the Seebeck voltage. Each TE element was divided into a discrete number of nodes in the direction of the heat flow from the hot to cold side and the temperature dependent Seebeck voltage at each node was calculated. The total Seebeck voltage was calculated by adding the individual Seebeck voltages. The total power is calculated by the expression:

$$P = I^2R_{load} \tag{4}$$

For a pair of thermoelectric legs with convection heat transfer on both sides and isothermal interconnects with negligible electrical heating, the boundary conditions are combined heat flux and temperature. The interconnects, which are typically copper, are assumed to be isothermal because the thermal conductivity is high. Generation due to Joule heating is assumed to be negligible due to high electrical conductivity, and thermoelectric energy conversion at the interface of the interconnects and the TE materials is neglected. On both the hot- and cold-side of the TE leg pair, the temperature of each leg must be equal to the temperature of the isothermal interconnect interface, and this is also the temperature driving the conduction heat flux. The total composite heat flow is given by:

$$Q_{comp} = A_nq_n + A_pq_p \tag{5}$$

where A is the cross-sectional area of the n- or p-type leg, Q_{comp} is the total composite heat flow, and q is the heat flux in the specified leg. A visual representation of the p-type, n-type and void areas is shown in Fig. 3. The void area is the empty space between adjacent TE legs, and it is assumed to be perfectly insulated.

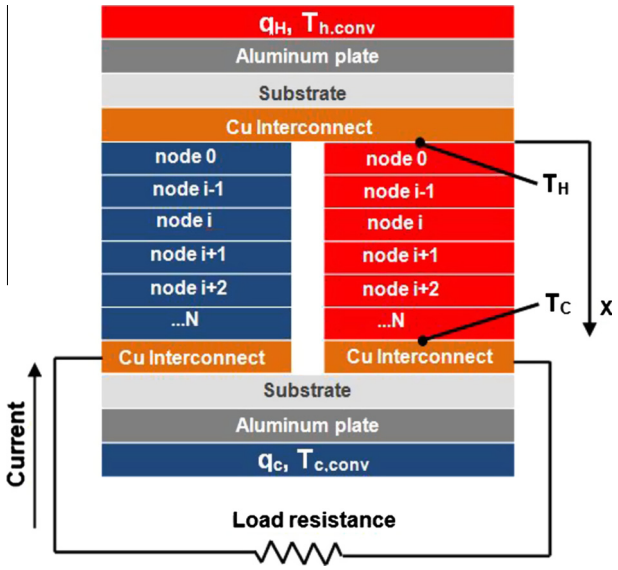

Fig. 2. Schematic of numerical scheme of TE leg pair.

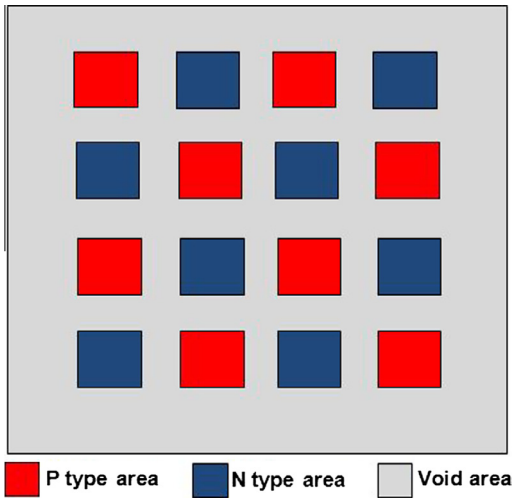

Fig. 3. Schematic of a TE leg layout areas with void space.

The total composite heat flow must be equal to the total heat flow to or from the hot and cold heat exchangers to/from either the hot or cold side of the TE element, given by,

$$Q_{h,comp} = \frac{(T_{h,conv} - T_h)}{R_h} \quad (6)$$

for the hot-side, and

$$Q_{c,comp} = \frac{(T_c - T_{c,conv})}{R_c} \quad (7)$$

for the cold-side, where R is the overall heat transfer resistance for the hot or cold side (including thermal resistance due to conduction and contact resistances associated with the aluminum plate, substrate, and interconnect as well as thermal resistance due to convection as shown in Fig. 4), T_{conv} is the temperature of the hot or cold fluid, T is the temperature of the hot or cold side of the TE leg pair, and Q_{comp} is the total composite heat flow on the hot or cold side of the TE device, given in Eq. (5). Subscripts h and c indicate whether the variable corresponds to the hot or cold side. The radiation heat loss from the TE elements at various operating temperatures and fill fractions was computed assuming the TE elements radiate as black bodies. The radiation heat loss from the TE leg surfaces for all cases was found to be less than 2% of the total heat input provided from the hot side. Therefore, radiation effects were neglected.

The temperature boundary conditions are specified as follows:

$$T_{n,h} = T_{p,h} = T_h \quad (8)$$

$$T_{n,c} = T_{p,c} = T_c \quad (9)$$

where as before, subscripts n and p indicate n- or p-type leg, and subscripts c and h indicate cold or hot side. The parameter used in this study to characterize the coverage of TE materials present in a given area of the module is termed the fill fraction, and is given by:

$$FF = fill\ fraction = \frac{A_n + A_p}{A_n + A_p + A_{void}} \quad (10)$$

3. Experimental validation

3.1. Device fabrication

Two different TE devices – the 1st and 2nd generation, each composed of a single TE leg pair were fabricated for the purpose of experimental model validation. The compositions of the TE elements used in the 1st and 2nd generation TE devices are shown in Table 1. The dimensions of the TE elements are listed in Table 2. The 1st generation TE device was assembled by bonding copper interconnects directly to the TE elements using a commercial silver paste with high thermal and electrical conductivity. The bonded piece was then sandwiched between electrically insulating and thermally conducting ceramic substrates. The TE elements were connected in series electrically and in parallel thermally.

Table 1
TE Materials used in 1st and 2nd generation TE device fabrication.

Material	Type	Composition
HMS	p-type	$Mn(Al_{0.0015}Si_{0.9985})_{1.8}$
MgSi	n-type	$Mg_2(Si_{0.4}Sn_{0.4}Ge_{0.2})_{0.985}Sb_{0.015}$

Table 2
Dimensions of TE legs used in 1st and 2nd generation TE devices.

Dimension	1st generation		2nd generation	
	p-Type	n-Type	p-Type	n-Type
Base area (mm^2)	5.22 × 5.42	4.52 × 5.26	5.48 × 5.35	5.56 × 5.65
Height (mm)	4.97	4.97	6.22	6.22

An improved 2nd generation TE device was constructed using a two-step SPS (Spark Plasma Sintering) process. First, the p-type and the n-type samples were prepared using SPS. In the second step, SPS was used again to bond copper electrodes to the TE elements. The sintering temperatures for the n-type and the p-type samples were 650 °C and 600 °C, respectively. Samples were then cut into rectangular blocks, and commercial silver paste was used to assemble the whole device. Unlike in the 1st generation TE device, where the commercial paste was used for Cu–TE element bonding, the paste was used in this case solely for Cu–Cu bonding. The device was then sandwiched between ceramic substrates. Photos of both the devices are shown in Fig. 5.

3.2. Electrical contact resistance measurement

The four probe measurement technique was used to measure the electrical resistance of TE elements as well as the contact resistances for the 1st and the 2nd generation TE devices. A small current was supplied from a constant current source and voltage drops at various locations on the TE devices were measured. The slope of I–V curve was taken as the electrical resistance. The experimental data for the 2nd generation device are shown in Fig. 6. The

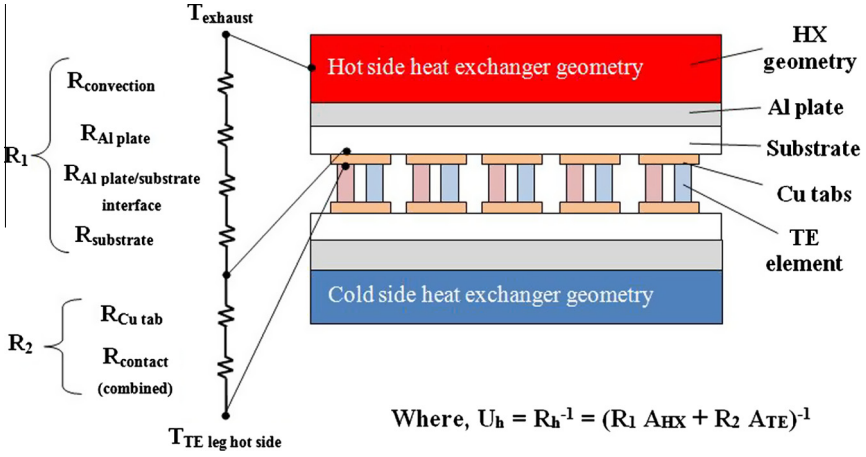

Fig. 4. System level integration of thermoelectric modules into the heat exchanger.

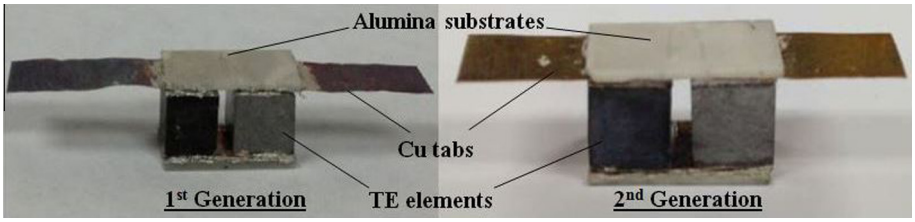

Fig. 5. The 1st generation TE device (left)was fabricated using commercial silver paste for electrode bonding while SPS was used for electrode bonding for the 2nd generation TE device (right).

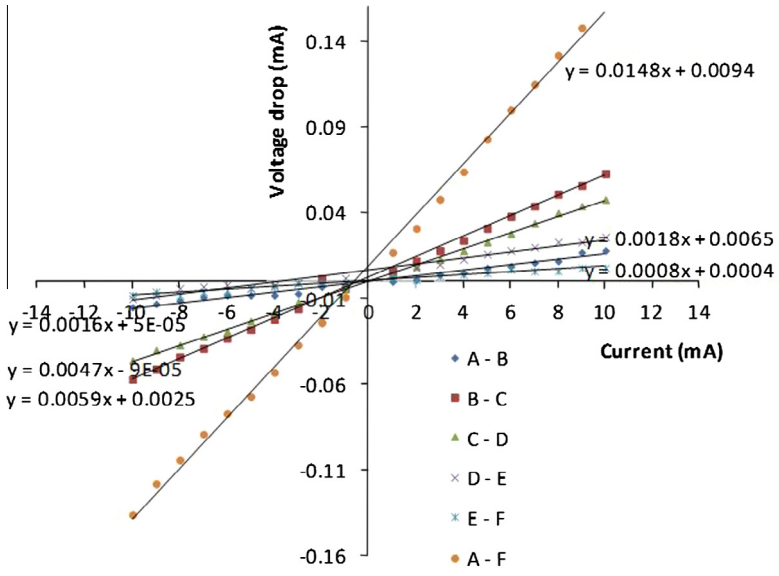

Fig. 6. Voltage drops between different locations on the 2nd generation TE device for various values of constant current flow. The slope of linear fit was used to derive resistance values. Refer to Fig. 7 for probe locations A through F.

different lines show measurements taken between different points in the TE circuit consisting of the two-element device and interconnects.

Fig. 7 shows the experimentally measured values of electrical resistance of the TE elements as well as the electrical contact resistance between the given elements of the devices. Temperatures of the hot and cold sides were recorded to account for Peltier heating. However, the temperature differences were negligible for the small current flows used. The results, as shown in Fig. 7, show a very large decrease of almost two orders of magnitude in contact resistance when the SPS technique was used for bonding the copper electrodes to TE elements versus bonding with the paste. The optimum sintering conditions for such bonding processes may be expected to vary for different TE materials. Finding the optimum SPS conditions can have an impact on the quality of bonding. Contact resistance can be decreased further by finding the optimum sintering conditions for electrode-TE element bonding. These data were incorporated into the device model which is discussed in the model validation section.

3.3. Power output measurement and model validation

An experimental setup was designed and constructed to validate the numerical TEG model. A one-dimensional heat flow device was made using a hot plate as the heat source and a circulating water heat exchanger as the heat sink. The TE device was placed in between the heating and the cooling sections. The heating and cooling sides were both thermally insulated to facilitate larger temperature drops across the TE devices.

The experimental setup is shown in Fig. 8. For various heating loads, the temperature readings of the hot sides and cold sides of both the TE elements were recorded using K-type and T-type thermocouple wires for the 1st generation and the 2nd generation TE devices, respectively. Open circuit voltage and the voltage drop across a load resistance were also measured. The numerical model was modified for the specified temperature boundary conditions for comparison with the experiments.

Fig. 9 shows the numerical and experimental electrical power output for both the 1st and 2nd generation TE devices as a function of the temperature difference between the hot and the cold sides. Power delivered by the TE device to the combined load resistance and contact resistance is plotted. Because of the significantly lower electrical contact resistance of the 2nd generation device, its power delivery was significantly greater than that of the 1st generation device. The numerical model under predicts the power output for the 1st and 2nd generation TE device by an average of 20% and 23%, respectively, over the range of temperatures measured. Because of heat loss from the surfaces of the TE elements (where the thermocouples were attached), the average hot and cold side temperatures measured are expected to be lower than the actual area average temperatures, such that the temperatures in the center were higher than the temperatures at the surface. In addition, because of geometrical constraints, the thermocouples were bonded to the sides of each TE element, a small distance away from the top and bottom of the TE element. Therefore, the temperature

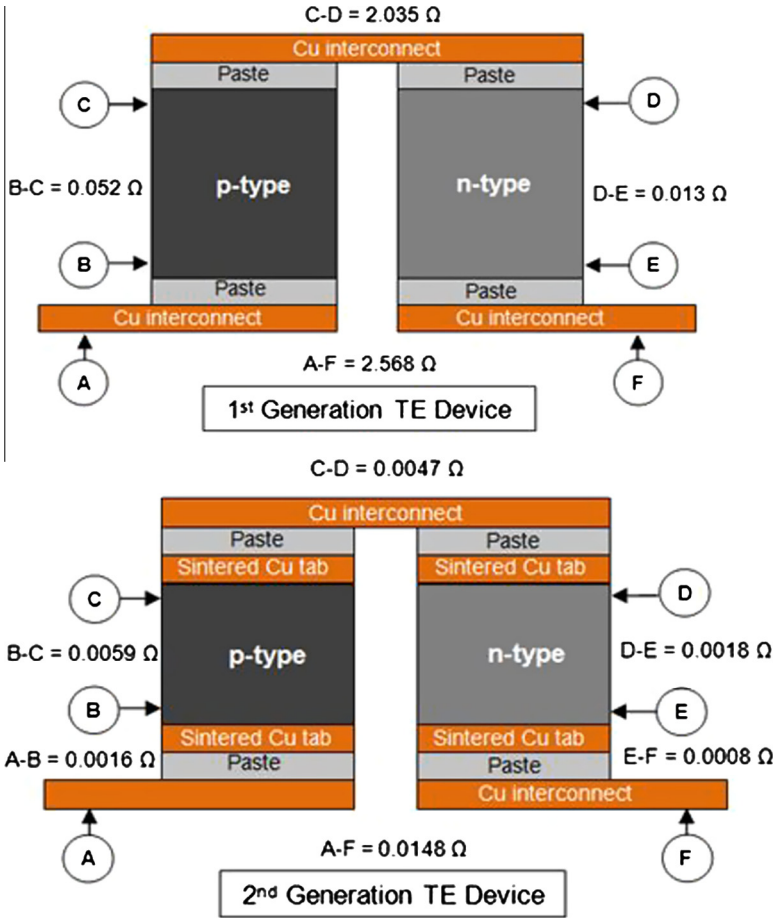

Fig. 7. Experimentally measured electrical resistance of constituting elements of the 1st generation TE device (left) and the 2nd generation TE device (right) in ohms. Total electrical resistance of the 1st device is 2.568 Ω and that of the 2nd is 0.0148 Ω.

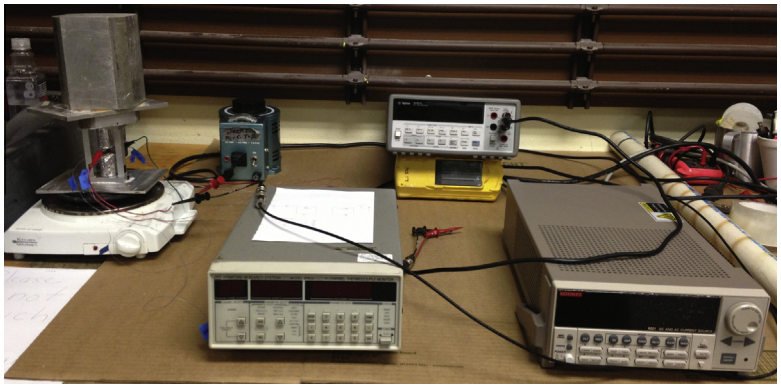

Fig. 8. Experimental setup for 1st and 2nd generation TE device power output measurement.

difference measured by thermocouples was slightly lower than the actual temperature difference across the entire TE element. Since the model calculates the Seebeck voltage and the corresponding power output based on the measured temperature difference, a lower temperature difference is expected to result in a lower Seebeck voltage and therefore lower power output.

The accuracy of the experimentally determined power depended on the measurements of voltage and load resistance. The uncertainty in the voltage measurements was ±0.0005 mV based on the accuracy of voltmeter. The load resistance was determined from the current and the measured voltage across the resistance. Based on the device accuracy, the load uncertainty in load resistance was ±0.001 mΩ. From these uncertainties, there was an average error of approximately 7.2% in experimental power output measurement over the range of data.

The power from the model relied on the Seebeck voltage calculated from the measured material Seebeck coefficient and the temperature difference across the TE element. The estimated uncertainty in the Seebeck coefficient was ±5%. The largest source of uncertainty in the model derived power was contributed by the uncertainty in the temperature gradients in the TE elements. While the uncertainty of the thermocouple measurements was

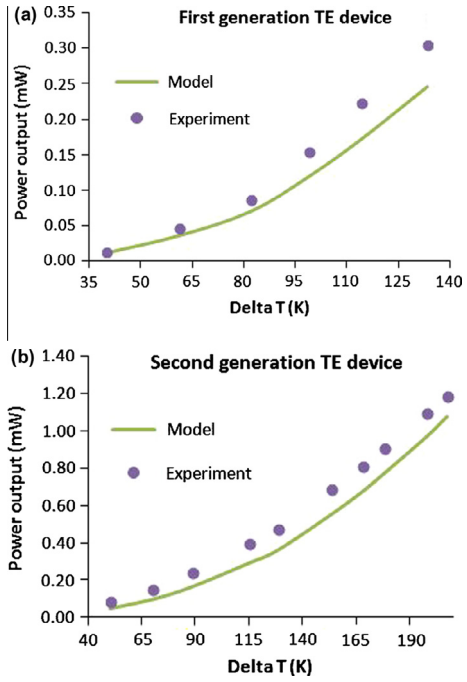

Fig. 9. Modeling and experimental results for power delivered to the electrical load for various temperature differences between the hot and cold sides of the TE elements for the 1st generation and the 2nd generation TE devices. The cold side temperatures were in the range of 315 K–421 K while the hot side temperatures varied in the range of 355 K–629 K.

Table 3
Summary of key parameters and results from the experimental study.

Parameter	1st Generation TE device	2nd Generation TE device
Hot side temperature range	370–519 K	401–687 K
Cold side temperature range	311–352 K	322–262 K
Maximum power output	0.30 mW (at ΔT = 133 K)	1.19 mW (at ΔT = 207 K)
Electrical resistance of the whole device	2.568 Ω	0.0148 Ω
Electrical contact resistance	2.503 Ω	0.0071 Ω

approximately ±2 K, the uncertainty in the axial location of thermocouples was about ±0.5 mm which contributed an effective uncertainty in temperature gradient of approximately 3% at each end. These uncertainties propagated yield an uncertainty in the model power of approximately ±12.5%, thus, the model uncertainties of power output were found larger than experimental values.

Unlike the 1st generation TE device, the Seebeck coefficients of the TE elements of the 2nd generation TE device were not the same as the properties measured on pure samples. The high temperatures in the SPS needed to sinter the copper electrodes to the TE elements resulted in diffusion of copper into the TE elements, forming silicides of copper. The Seebeck coefficients of the TE elements after sintering them with copper electrodes was measured to be about 70% of the original value. One of the disadvantages of sintering electrodes to the TE materials is that a barrier material needs to be used to minimize diffusion. The characteristics of several barrier materials which may be applicable to silicide TE materials are currently being studied. Important parameters and findings of the experiment have been summarized in Table 3.

4. Model results

As mentioned above, four parameters, leg length, fill fraction, leg area ratio, and load resistance were considered for optimization

Table 4
Specified boundary conditions for this study. These are typical values for coolant and exhaust averaged in the stream-wise direction.

Parameter	Value
Hot side convection temperature	600–800 K
Cold side convection temperature	300 K
Hot side overall convection coefficient	2.0 kW/m^2 K
Cold side overall convection coefficient	8.0 kW/m^2 K

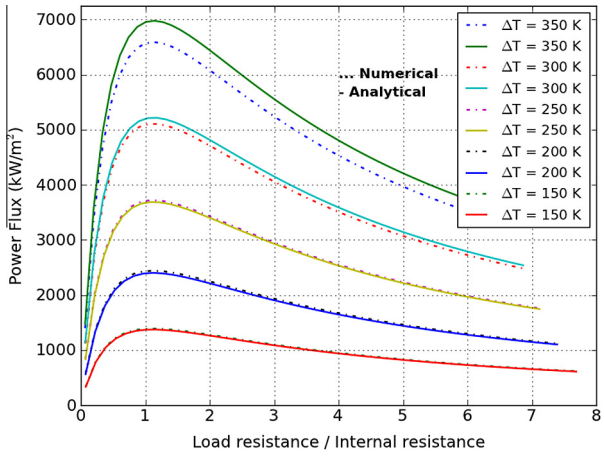

Fig. 10. The effect of load resistance on the power produced per unit area of the TEG module. Maximum power flux is produced when the electrical load resistance is equal to the internal resistance. Cold side convection boundary condition is kept constant at 300 K.

of a TEG. Boundary conditions used for this modeling study are listed in Table 4. To simulate a typical finned heat exchanger geometry, the overall heat transfer coefficients averaged in the streamwise direction for both the hot and cold sides were used, as previously reported by Baker et al. [33]. These numbers were reported for a heat exchanger installed in the exhaust of a Cummins 6.7 L diesel engine. In the model, the heat exchanger was discretized in the flow direction as 25 individual streamwise sections. While the hot-side temperature fell approximately logarithmically in the flow direction, the hot-side temperature was taken as constant over the extent of each of the sections at the average value for that section [33]. The thermal efficiency resulting from the optimization study of TEG devices presented in this study was approximately 3.8%.

All four parameters require optimization to achieve the maximum power flux. The results showed that the sensitivities could be very different among the parameters, however, it was found that the maximum power flux remained in a narrow range of leg area ratio between n-type and p-type legs even as the other three parameters varied widely. This is because the temperature dependency of the TE properties exhibited a similar trend for both the n-type and p-type materials. For the boundary conditions provided in Table 4, the leg area ratio between n-type and p-type legs was fixed at 0.42 based on the optimization results. In contrast, for conventional bismuth telluride TE materials, the leg area ratio was found to be roughly unity. An analytical value for this ratio can be estimated using the equation [32],

$$\frac{A_n}{A_p} = \sqrt{\frac{\rho_n k_p}{\rho_p k_n}} \tag{11}$$

This equation estimates an optimum leg area ratio of 0.46 between n-type and p-type legs. However, this optimal area ratio is based on an averaged values of ρ and k for the given hot- and

cold-side temperatures. For the given boundary conditions and range of operating temperatures, theoretical analysis slightly over-predicts the optimum leg area ratio by approximately 10%.

The variation of net power flux output $P_{flux,out}$ for a TEG module at different values of electrical load resistance is shown in Fig. 10. The x-axis has been normalized by the internal resistance of the module. Maximum power flux is achieved at a load resistance nearly equal to the internal resistance of the module. For load resistance below this optimum value, there is a steep drop in the power output as load resistance decreases. The decrease is more gradual with increasing load resistance; this behavior would have implications for specifying load resistance for a practical system where it would be desirable for the available power to be less sensitive to load resistance. Without accounting for the temperature dependence of the TE properties, an analytical expression representing power flux output as a function of resistance ratio, m', is [32],

$$P_{flux,out} = \frac{P_{out}}{Area} = \frac{\left[(\alpha_p - \alpha_n)\left(T_{Hot,leg} - T_{Cold,leg}\right)\right]^2 m'}{(1+m')^2 R_{internal}} \frac{1}{Area} \tag{12}$$

For a given temperature difference, length, and cross sectional area of TE legs, the power flux output is plotted against electrical resistance ratio for both based on this analytical expression and for the model, in Fig. 10.

It is clear from Fig. 10 that the theoretical and numerical results follow the same trends. However, the analytical solution slightly over-predicts the power flux compared to the numerical solution. This is because the numerical solution uses temperature dependent TE properties as opposed to temperature averaged TE properties used in theoretical analysis. This discrepancy can be attributed to the non-linear dependence of ZT on temperature for the silicides under consideration. For temperature differences less than 400 K, the differences in predicted power flux between the analytical and numerical model are small, but they increase with increasing temperature difference such that the analytical model may over-predict power by more than 10% for a 500 K temperature difference.

Two different cases regarding the thermal circuit shown in Fig. 4 have been considered in the present study. In the first case, the model assumption is that the thermal contact resistance between the TE elements and the heat exchanger is negligible. This does not include the contact resistance between the aluminum plate and the substrate, which has been included in R_1 as shown in Fig. 4. Thermal contact resistance between the aluminum plate and the substrate has been taken as a constant throughout this study. This first case is an ideal case where parasitic thermal contact resistance between the two was not considered ($R_2 = 0$ in Fig. 4). For the second case, the thermal resistance due to the contact resistance between various constituting layers such as the metal interconnects and electrically insulating ceramic substrates was included in the model. Contact resistance has been found to be a strong function of operating temperature, clamping pressure, surface finish, and material composition, among other variables

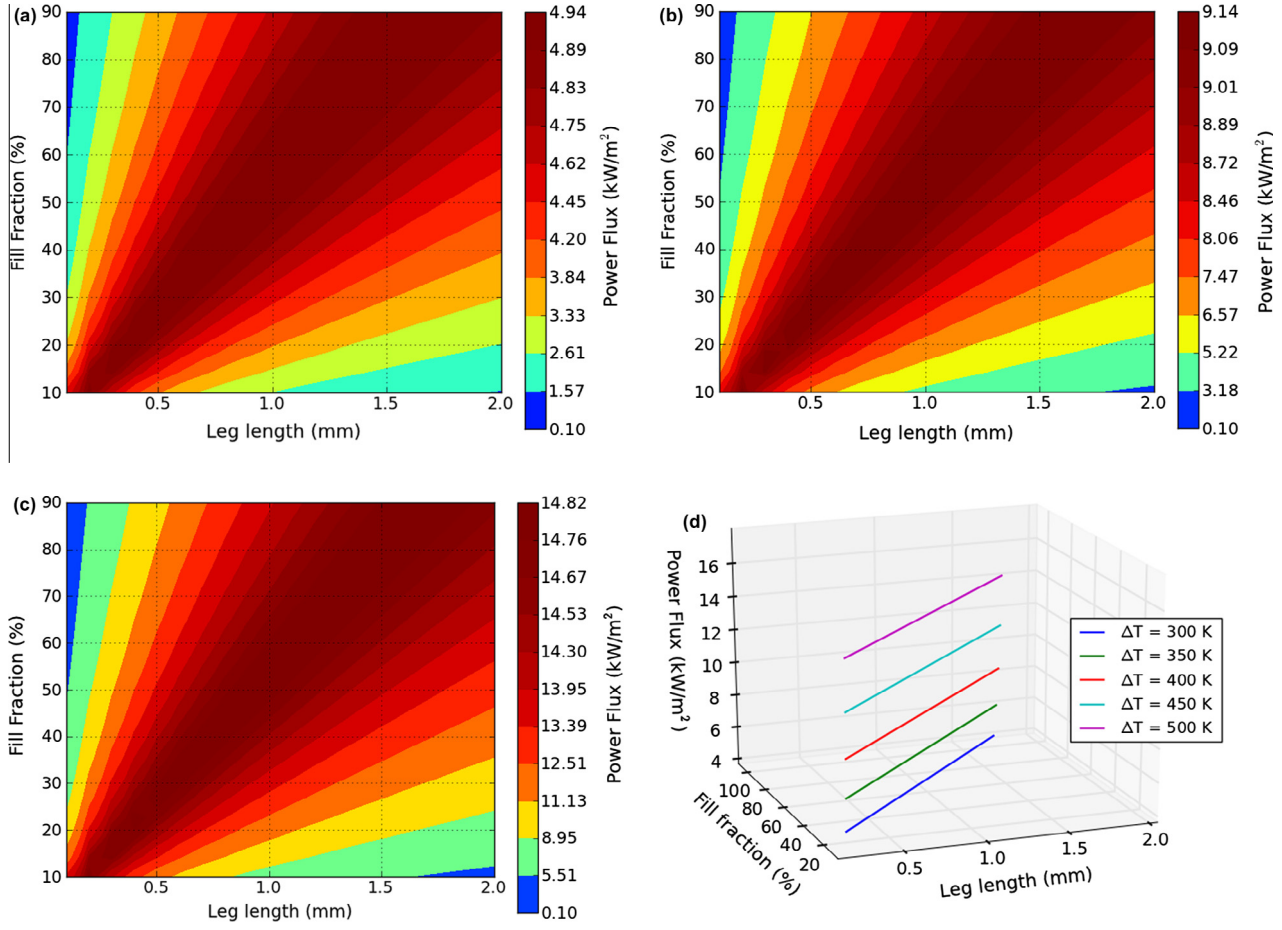

Fig. 11. Contours of peak power flux for a TEG module plotted against fill fraction and leg length for negligible thermal contact resistance case. The leg area ratio between the n-type and p-type legs is optimized and fixed at 0.42, and the electrical load resistance for each case is equal to the internal resistance. Results have been shown for a temperature difference between the exhaust and the coolant of 300 K, 400 K, and 500 K between the exhaust and the coolant in (a–c) respectively. (d) Summarizes the results from (a–c).

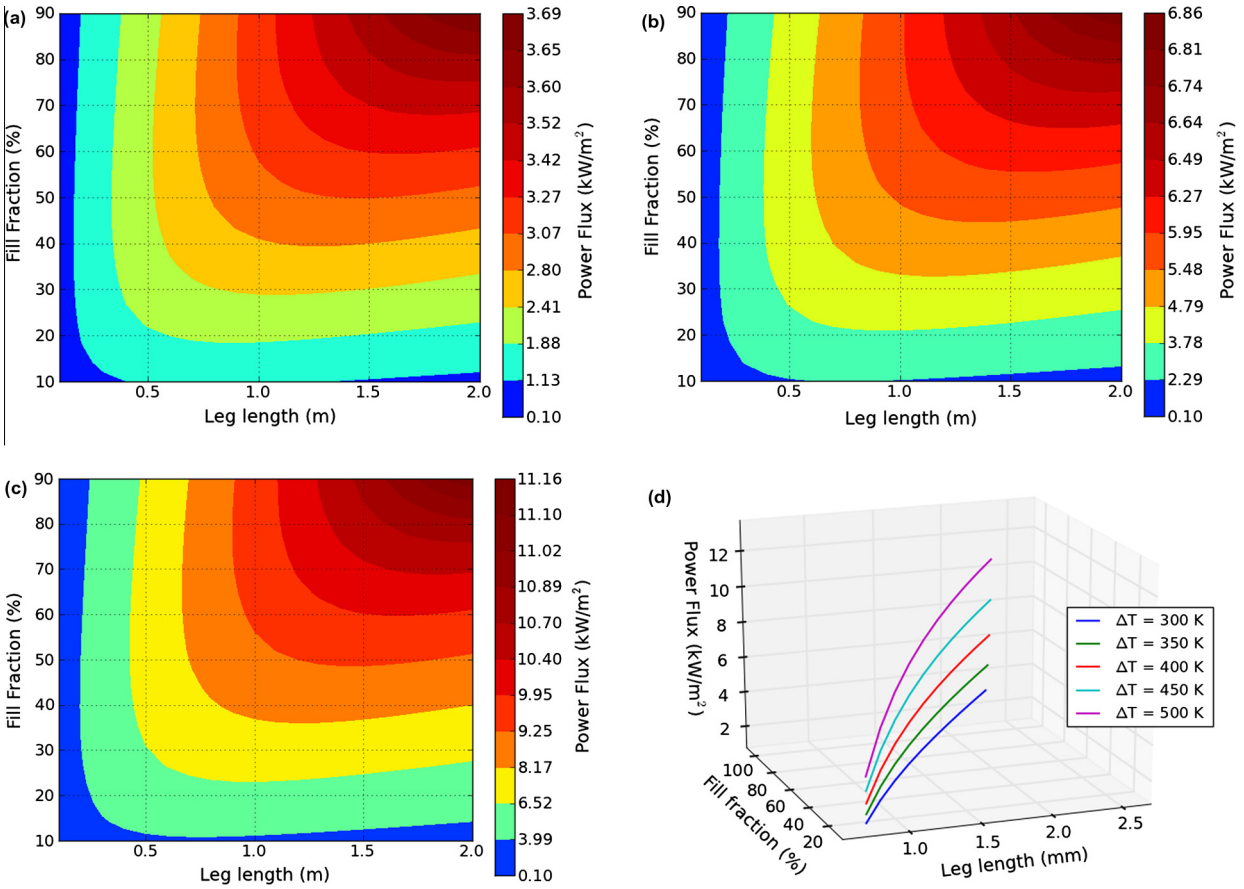

Fig. 12. Contours of peak power flux for a TEG module plotted against fill fraction and leg length when thermal contact resistance is included into the model. The leg area ratio between the n-type and p-type legs is optimized and fixed at 0.42, and the electrical load resistance for each case is equal to the internal resistance. Results have been shown for a temperature difference between the exhaust and the coolant of 300 K, 400 K, and 500 K between the exhaust and the coolant in Fig. 11(a–c) respectively. Fig. 11(d) Summarizes the results from Fig. 11(a–c).

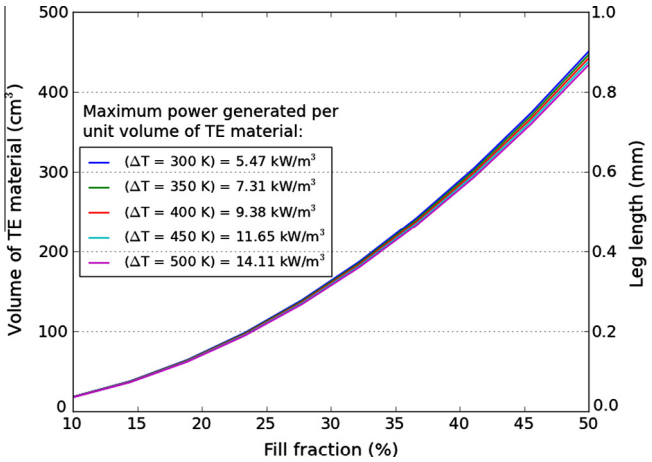

Fig. 13. Volume of TE material per m^2 and optimum leg length for optimal power flux vs. Fill fraction at various TE leg temperature differences.

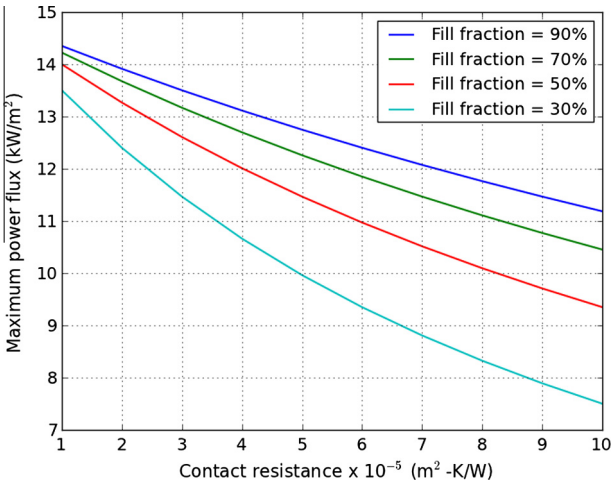

Fig. 14. Peak power flux is plotted against total contact resistance of a module for various fill fractions and the range of contact resistance considered in this study.

[34–36]. After a comprehensive literature review, a combined contact resistance in the range of 0.0001 m^2 K/W and 0.00001 m^2 K/W was considered reasonable for modeling purposes in this study (R_2 = 0.0001–0.00001 m^2 K/W in Fig. 4).

Modeling results for the two cases are shown in Figs. 11 and 12, respectively. For the first case, which characterizes an ideal scenario where the thermal resistance between the TE elements and the exchangers is negligible, the optimization results are shown in Fig. 11(a–d). A very important observation made in this case is that there are multiple solutions in the geometrical optimization of TEG modules. Various combinations of optimal leg length, fill fraction, leg area ratio, and load resistance (or current) can be achieved, which provide the same theoretical peak power flux, given model assumptions. As discussed earlier, the leg area ratio and the ratio of electrical load resistance to internal resistance

for peak power flux output are 0.42 and unity, respectively. Fig. 11(a–c) provide contour plots which show the optimization results for temperatures differences of 300 K, 400 K, and 500 K, respectively. For a given temperature difference, these contour plots show that the maximum power output is achievable at all fill fractions, as long as the leg length is optimized, too. In other words, the ratio of fill fraction to leg length is kept constant. This plot illustrates that fewer legs, i.e., a small fill fraction-with legs of shorter length have the potential to achieve the same peak power flux output as a greater number of longer legs, when integrated into a heat exchanger. Essentially, a smaller volume of TE material can provide the same power flux, given the geometrical configuration is accurately optimized. This is shown in the Fig. 13 where the volume of TE materials is plotted against fill fraction for optimal cases. For example, the same power flux can be produced with 40 cm^3 of TE material as with 400 cm^3 of material per m^2 heat exchanger area. The relationship between fill fraction and leg length that results in optimal TEG performance presented in this study is consistent with the results of Gomez et al. [29]. Results for various temperature differences are summarized in Fig. 11(d).

For the second case, where contact resistance between the TE elements and the hot- and cold-side heat exchangers is included in the model, the optimization results are shown in Fig. 12. Similar to Fig. 11, contour plots for temperature differences of 300 K, 400 K, and 500 K, respectively, were produced for this case, as well. Peak power flux output was plotted against leg length and fill fraction for various temperature differences between the exhaust and the coolant as summarized in Fig. 12(d). The plots show that the power output increases as fill fraction and leg length are both increased. This shows that a greater number, i.e., larger fill fraction-of longer legs produces greater power output than fewer short legs, when the contact resistance is taken into account. It is desirable to maximize the temperature drop across the TE elements for peak power output. For a given heat flux extracted from the exhaust gas at specified exhaust and coolant temperatures, the total thermal resistance in between has to stay the same. Increasing the fill fraction, and hence the contact area, leads to smaller contact resistance. This allows for the thermal resistance of the TE elements to increase by increasing their length. The total thermal resistance is still the same, but the temperature drop across the TE elements is larger because of their greater thermal resistance. This conclusion is relevant to the practical application of such TE devices where thermal contact resistance can be a major design parameter.

For exhaust and coolant temperatures of 800 K and 300 K respectively, the peak power output for the case where parasitic thermal contact resistance between the TE elements and the heat exchangers is considered negligible is predicted to be 14.8 kW/m^2. Fig. 14 shows the sensitivity of peak power to the thermal contact resistance for the proposed range of contact resistance. At higher fill fractions, for instance, 90%, peak power is almost linearly dependent on contact resistance. For lower fill fractions, the dependence is nonlinear. According to the results, for a 50% fill fraction, incorporating a parasitic resistance of 0.00001 m^2 K/W between the TE elements and the heat exchanger on each side drops the peak power output by 1.2% to 13.9 kW/m^2; increasing the parasitic resistance to 0.0001 m^2 K/W reduces the peak power output by nearly 36%. Key parameters and findings for the modeling study have been summarized in Table 5.

Table 5
Summary of key parameters and results from the modeling study.

Parameter	Value
Cold side temperature	300 K
Hot side temperature	500–800 K
Hot side overall heat transfer coefficient	2.0 kW/m^2 K
Cold side overall heat transfer coefficient	8.0 kW/m^2 K
Contact resistance considered for the study	0.0001–0.00001 m^2 K/W
Maximum theoretical power per m^2	14.8 kW/m^2 (no contact resistance)
Peak thermal efficiency	3.8%
Leg area ratio (n-type/p-type)	0.42
Internal electrical resistance to load resistance ratio	~1

5. Conclusions

This paper introduces a numerical model for predicting power output of thermoelectric heat exchangers using specified convection and temperature boundary conditions. The study was carried out for a heat exchanger installed in the exhaust of a Cummins 6.7 L diesel engine designed for TEG modules that are to use Mg_2Si and p-type $MnSi_{1.8}$ based silicides as TE materials. The model was used to optimize TEG module fill fraction, leg length of TE elements, leg area ratio between n- and p- type legs, and load resistance. The 1st and 2nd generation TE pair devices were designed and fabricated using Mg and Mn silicides to experimentally validate the model. A large improvement in electrical contact resistance was observed when the SPS technique was used to perform the TE element – Cu electrode bonding compared to using a highly conductive commercial silver paste. The electrical contact resistance for a single TE pair device was measured to be 2.503 Ω and 0.0071 Ω for the 1st and 2nd generation TE devices, respectively. These values were incorporated into the numerical model for model validation.

Two different cases were considered for the numerical TE device model. For the first case, the thermal contact resistance between the TE elements and the heat exchangers, was considered to be negligible. For this case the optimization study concluded that a smaller number of shorter legs are capable of producing the same power per unit module area as a greater number of longer legs. The numerical model predicted a maximum power generation of 14.8 kW/m^2 for exhaust and coolant temperatures of 800 K and 300 K respectively.

For the second case, the thermal contact resistance was incorporated into the model to simulate realistic operating conditions. For this case, it was observed that a greater number of longer legs will produce higher power than fewer short legs. The peak power output increased with increasing TE leg length and fill fraction. At 90% fill fraction, the peak power output was 11.18 kW/m^2 for exhaust and coolant temperatures of 800 K and 300 K, respectively. Inclusion of thermal contact resistance in the model predicted a drop in peak power of 1.2% and 36% for contact resistances of 0.00001 m^2 K/W and 0.0001 m^2 K/W, respectively.

For both cases, optimum leg area ratio between n- and p-type legs was determined to be 0.42 for exhaust gas temperatures of 600–800 K and coolant temperature of 300 K. A load resistance nearly equal to the internal resistance of the module was found to produce maximum power per unit area of the heat exchanger.

Acknowledgements

This project was carried out under a grant from the NSF/DOE Joint Thermoelectric Partnership, award number CBET-1048767. Libin Zhang and Xi Chen are thanked for their help in preparing the silicide thermoelectric materials used in the experiments.

References

[1] Heywood John. Internal combustion engine fundamentals. McGraw-Hill; 1988.
[2] Caton JA. Operating characteristics of a spark-ignition engine using the second law of thermodynamics: effects of speed and load. SAE Technical Paper; 2002. p. 2000-01–0952.

[3] Endo T, Kawajiri S, Kojima Y, Takahashi K, Baba T, Ibaraki S, Taka- hashi T, Shinohara M. Study on maximizing energy in automotive engines. In: Technical Report 2007-01-0257. Warrendale, PA: SAE International; April 2007.
[4] Miller Erik W, Hendricks Terry J, Peterson Richard B. Modeling energy recovery using thermoelectric conversion integrated with an organic rankine bottoming cycle. J Electron Mater 2009;38(7):1206–13.
[5] Weerasinghe WMSR, Stobart RK, Hounsham SM. Thermal efficiency improvement in high output diesel engines a comparison of a rankine cycle with turbo-compounding. Appl Therm Eng 2010;30(14–15):2253–6.
[6] Talom Hugues L, Beyene Asfaw. Heat recovery from automotive engine. Appl Therm Eng 2009;29(2–3):439–44.
[7] Hendricks TJ, Lustbader JA. Advanced thermoelectric power system investigations for light-duty and heavy duty applications II. Thermoelect IEEE 2002:387–94.
[8] Hussain E Quazi, Brigham R David, Maranville W Clay. Thermoelectric exhaust heat recovery for hybrid vehicles. Technical Report 2009–01-1327. Warrendale, PA: SAE International; April 2009.
[9] Crane Douglas, Jackson Gregory, Holloway David. Towards optimization of automotive waste heat recovery using thermoelectrics. Technical Report 2001–01-1021. Warrendale, PA: SAE International; March 2001.
[10] Hendricks TJ. Thermal system interactions in optimizing advanced thermoelectric energy recovery systems. J Energy Res Technol 2007;129:223–31.
[11] LaGrandeur John W, Bell Lon E, Crane Douglas T. Recent progress in thermoelectric power generation systems for commercial applications. MRS Spring meeting; 2011.
[12] Yang. In: Proceedings of 24th international conference on thermoelectrics (ICT); 2005. p. 170–4.
[13] Rowe DM. Int J Innovations Energy Syst Power 2006;1:13.
[14] Rowe DM. CRC handbook of thermoelectrics. CRC Press; 1995. p. 441–58.
[15] Stobart Richard, Milner Dan. The potential for thermoelectric regeneration of energy in vehicles. Technical Report 2009-01-1333, Warrendale, PA: SAE International; April 2009.
[16] Stobart K Richard, Wijewardane Anusha, Allen Chris. The potential for thermoelectric devices in passenger vehicle applications. Technical Report 2010–01-0833, Warrendale, PA: SAE International; April 2010.
[17] Omer SA, Infield DG. Design optimization of thermoelectric devices for solar power generation. Sol Energy Mater Sol Cells 1998;53:67–82.
[18] Xuan XC. Optimum design of a thermoelectric design. Semicond Sci Technol 2002;17:114–9.
[19] Cheng Yi-Hsiang, Lin Wei-Keng. Geometric optimization of thermoelectric coolers in a confined volume using genetic algorithms. Appl Therm Eng 2005;25:2983–97.
[20] Wang Yuchao, Dai Chuanshan, Wang Shixue. Theoretical analysis of a thermoelectric generator using exhaust gas of vehicles as heat source. Appl Energy 2013;112:1171–80. ISSN 0306-2619.
[21] Chen Lingen, Li Jun, Sun Fengrui, Wu Chih. Performance optimization of a two-stage semiconductor thermoelectric-generator. Appl Energy 2005;82(4):300–12. ISSN 0306-2619.
[22] Gou Xiaolong, Xiao Heng, Yang Suwen. Modeling, experimental study and optimization on low-temperature waste heat thermoelectric generator system. Appl Energy 2010;87(10):3131–6.
[23] Matsubara K, In: Proceedings of 21st international conference on thermoelectrics (ICT); 2002. p. 418–23.
[24] Kushch AS, Bass J, Ghamaty S, Elsner N. Thermoelectric development at Hi-Z technology. In: 20th international conference on thermoelectrics; 2001.
[25] Crane Doug T. An introduction to system level steady-state and transient modeling and optimization of high power density thermoelectric generator devices made of segmented thermoelectric elements. J Electron Mater 2011;40(5):561–9.
[26] Crane Douglas T, Jackson Gregory S. Optimization of cross flow heat exchangers for thermoelectric waste heat recovery. Energy Convers Manage 2004;45(9–10):1565–82.
[27] Kumar, Sumeet, Heister, Stephen, Xu, Xianfan, et al. Thermoelectric generators for automotive waste heat recovery systems. Part I: Numerical modeling and baseline model analysis. J Electron Mater 2013;42(4).
[28] Espinoza N, Lazard M, Aixala L, Scherrer H. Modeling a Thermoelectric generator applied to diesel automotive heat recovery. J Electron Mater 2010;39(9).
[29] Gomez M, Reid R, Ohara B, Lee H. Influence of electrical current variance and thermal resistances on optimum working conditions and geometry for thermoelectric energy harvesting. J Appl Phys 2013;113:174908.
[30] Chen X, Weathers A, Moore A, Zhou JS, Shi L. Thermoelectric properties of cold-pressed higher manganese silicides for waste heat recovery. J Electron Mater 2012;41:1564.
[31] Hogan TP, Shih T. Modeling and characterization of power generation modules based on bulk materials. Boca Raton (FL): CRC Press; 2006.
[32] Angrist W. Angrist. Direct Energy Conversion, Carnegie-Mellon University. 1977.
[33] Baker C. Simulation, design, and experimental characterization of catalytic and thermoelectric systems for removing emissions and recovering waste energy from engine exhaust. The University of Texas at Austin; 2012.
[34] Shi Ling, Wu Gang, et al. Interfacial thermal contact resistance between aluminum nitride and copper at cryogenic temperatures. Heat Mass Trans 2012;48:999–1004.
[35] Yovanovich M, Culham JR, Teertstra P. Microelectronics Heat Transfer Laboratory. Department of Mechanical Engineering: University of Waterloo; 1997.
[36] Satre V, Lallemand M. Enhancement of thermal contact conductance for electronic systems. Appl Therm Eng 2001;21:221–35.